Radio frequency attenuation by a rocket plume using diffraction theory and finite element modeling

Éva Dieudonné, Abelin Kameni, Lionel Pichon, David Monchaux

Radio frequency attenuation by a rocket plume using diffraction theory and finite element modeling

Éva Dieudonné[a,b,*], Abelin Kameni[a], Lionel Pichon[a], David Monchaux[b]

[a] *CentraleSupélec, Univ. Paris-Sud, Université Paris-Saclay, Sorbonne Universités, UPMC Univ Paris 06*
3 & 11, rue Joliot-Curie, Plateau de Moulon 91192 Gif-sur-Yvette CEDEX, France
[b] *CNES-DLA — Centre National d'Études Spatiales - Direction des lanceurs*
52, rue Jacques Hillairet 75612 Paris CEDEX, France

Abstract

Radio frequency communication between the space launcher and the mission control are unusually disturbed by the exhaust plume present in rocket engines. This paper presents the computation of radio wave propagation through the exhaust plume. Thus, frequency-domain finite element method and time-domain discontinuous Galerkin method are implemented for computations in case of a ground domain experiment. Numerical results compared to those obtained from ground experiment show good approximation of the propagation through the plasma over a wide frequency band. For the launcher in flight, an asymptotic method is proposed and has the advantage to give a fast evaluation of the scattering solution. In this case, the exhaust plume area is considered as a perfectly conducting trapezium whose parameters are extracted from the distribution of the plasma permittivity. Results related to the asymptotic method appear to be in good agreement with results based on the full wave approaches.

Keywords: Asymptotic method, electromagnetic, finite element, plasma, rocket plume, scattering.

*Corresponding author
Email address: evadieudonne@outlook.fr (Éva Dieudonné)

1. Introduction

During a space flight, it is crucial to ensure and maintain the radio frequency (RF) communications between the launcher and the mission control. The high quality reception of radio waves is very important to guarantee security during the flight. Unfortunately, the propagation of emitted and received waves is disturbed by the exhaust plume from the solid rocket motor of the launcher. Corrective measures can be established but are expensive. So, the interest of a sufficiently accurate predictive model is obvious.

The exhaust plume from the space launcher is an inhomogeneous plasma whose behavior can be studied through computational fluid dynamic (CFD) models described by Navier-Stokes's and Vlasov's equations [1, 2, 3, 4]. The plasma characteristics such as the permittivity, the collision frequency and the plasma frequency are deduced from those CFD models. Generally a frequency dependence of the permittivity is assumed and introduced in the Maxwell's equations whose resolution allows determining attenuation of RF transmission.

Today, only few works are dedicated to study RF transmission during a space flight [5, 6, 7, 8]. Kinefuchi's team has proposed to compute attenuation of RF waves by the plume in the cases of the ground experiment and the launcher in flight [5, 9, 10]. These works deal with all problems of jet impact on radio communications by addressing both, the chemical reactions within the engine, the CFD analysis of the plasma, and the electromagnetic interaction. The Fromentin-Denozière team's works also combine these different aspects to describe the electromagnetic signature of rocket engine plumes [8]. In this paper, aerothermochemical properties of the plume are computed and electromagnetic signature is obtained thanks to the study of the wave reflected by the plasma.

In these studies, numerical models of electromagnetic interaction are based on Finite Difference Time Domain method (FDTD). The computational domain is formed by the plasma whose shape has an important impact on the results. In case of simple shapes of the plasma, the FDTD method gives satisfactory results. Unfortunately practical rocket plumes are of arbitrary shape and the

use of a stair-case mesh in FDTD method may lead to significant errors.

Numerical calculation in 3D need RAM intensively and are time consuming. In [5] it was shown that 2D calculation are sufficient for the description of physical phenomena. In a 2D approach the electric field has only one component (out of plane component, z-component). However high frequency calculations corresponding to the case where the wavelength is small compared to the size of the plasma region still lead to heavy computational costs. It is why, in this case, an asymptotic method can be used for the prediction of the far field. Such diffraction method has been described in [11]. It considers that the far field scattered by the plasma is similar to the far field scattered by a perfectly conducting trapezium.

In this paper the attenuation of the radio frequency communication by a rocket plume of a space launcher is studied with 2D different methods. Two numerical discretization techniques are used for the computations: a frequency domain finite element method and a time domain discontinuous Galerkin method. Both of these methods are suited for unstructured meshes able to take into account arbitrary shapes of the rocket plume. They provide adequate tools for lowest frequencies. For high frequencies an asymptotic method has been developed using [12, 13, 14] and considers the plasma as a perfect conducting trapezium whose geometrical parameters are deduced from the distribution of permittivity.

2. Electromagnetic properties of plasma

The jet produced by the solid engine of the space launcher is an electron-rich plasma. Two trends will oppose and allow the plasma to remain in ionized form, while remaining globally neutral (quasi-neutrality). A tendency to disorder due to thermal agitation which will cause interactions between particles (collision or reaction) and a tendency towards organization through the collective aspect that manifests itself by the Coulomb interaction. From the study of these two trends, it is possible to define the plasma pulsation ω_p and the collision frequency ν_e.

The plasma frequency reflects the collective character of the Coulomb forces. The definition of ω_p describes a linear restoring force. Although this restoring force tends to restore the neutrality of the plasma, the result is an oscillation around the position ensuring neutrality.

The frequency of collision reflects the thermal agitation through the interaction of the particles. Since electrons are the fastest particles and our plasma is classified as cold plasma, we can assume that only electrons move in the plasma.

The article [7] shows that the plasma can be described by the parameters ω_p and ν_e with a permittivity given by equation (1).

$$\varepsilon_r(\omega) = 1 - \frac{\omega_p^2}{\omega\left(\omega - \imath\nu_e\right)} \tag{1}$$

where ν_e is the electron collision frequency (s^{-1}), ω_p the plasma frequency (s^{-1}) and ω the frequency ($\omega = 2\pi f$, s^{-1}).

The plasma frequency describes the frequency at which the electron density varies in the plasma. It is given by the equation (2).

$$\omega_p = \sqrt{\frac{N_e q_e^2}{\varepsilon_0 m_e}} \tag{2}$$

where N_e is electron density (m^{-3}), q_e is elementary electric charge ($1.602 \cdot 10^{-19}$ A·s), m_e is mass of an electron ($9.109 \cdot 10^{-31}$ kg), and ε_0 is permittivity of vacuum ($(36\pi \cdot 10^9)^{-1}$ $\mathrm{s}^4{\cdot}\mathrm{A}^2{\cdot}\mathrm{kg}^{-1}{\cdot}\mathrm{m}^{-3}$).

The electron collision frequency is the probability of collision between an electron and another species. It is given by equation (3).

$$\nu_e = \sum_j N_j Q_{ej} \sqrt{\frac{8 k_b T_e}{\pi m_e}} \tag{3}$$

where N_j is the density of species j (m^{-3}), Q_{ej} is the collision cross-section between a species j and an electron (m^2), k_b is Boltzmann constant ($1.38 \cdot 10^{-23}$ $\mathrm{m}^2{\cdot}\mathrm{kg}{\cdot}\mathrm{K}^{-1}{\cdot}\mathrm{s}^{-2}$), T_e is electron temperature (K).

3. Ground experiment

3.1. Configuration study

The ground experiment carried out by Kinefuchi team consists of two antennas placed on each side of the path of the exhaust plume from a rocket motor as in figure 1.

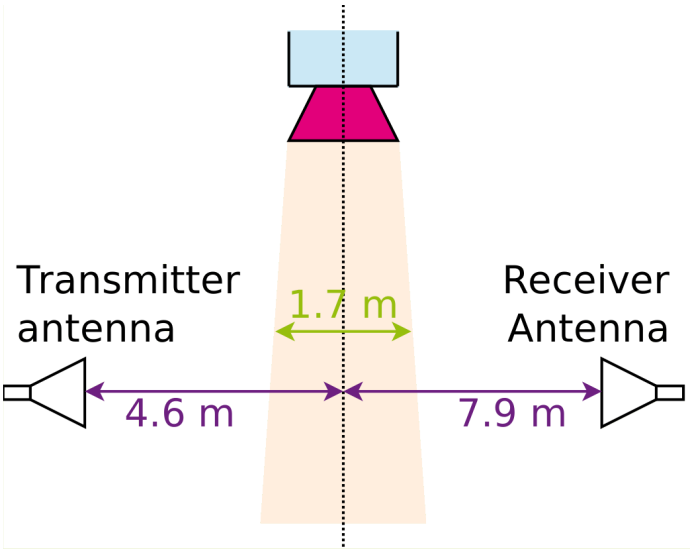

Figure 1: Kinefuchi antenna setup in ground experiment (Figure 2 in [10]).

A source antenna is placed at a distance of 4.6 m and a receiving antenna is placed at 7.9 m. The thickness of the plasma is 1.7 m. The field is recorded versus time in order to divide the engine firing period into periods with distinct electromagnetic properties. According to the work of [10], the firing period is divided into three durations: early period (10-20 s), middle period (40-50 s), and last period (95-105 s).

The normalized diffracted field is obtained by the ratio between z-component of electric field E in the presence of the plasma and z-component of electric field E_0 without plasma: $|E/E_0|$ (Table 3 in [10],Table 3).

3.2. Estimation of the parameters ω_p and ν_e

The method used in Kinefuchi's works to estimated the parameters ω_p and ν_e, from experimental results is not described in [10]. In this work, we propose a method to obtain a homogeneous parameters ω_p and ν_e from experimental data found in Kinefuchi's works [10].

Let define the attenuation L_{dB} (in dB) from the normalized scattered field E/E_0 as:

$$L_{dB} = -20 \log_{10} \left(\left| \frac{E}{E_0} \right| \right) \tag{4}$$

Assuming that the plasma is a layer of thickness y, reflection is negligible compared to attenuation and under normal incident wave, it is possible to express E/E_0 in the following form:

$$\frac{E}{E_0} = \exp\left(-\imath \frac{\omega}{c} \sqrt{\varepsilon_r} y \right) \tag{5}$$

So L_{dB} can be written in this form (in $\mathrm{m^2 \cdot s^{-1}}$), even if $\omega_p^2/(\omega^2 + \nu_e^2)$ is smaller than 1:

$$L_{dB} = 4.6 \cdot 10^{-5} \left(\frac{N_e \nu_e y}{\omega^2 + \nu_e^2} \right) \tag{6}$$

This expression can be found in [2] (equation 14) in $\mathrm{cm^2 \cdot s^{-1}}$.

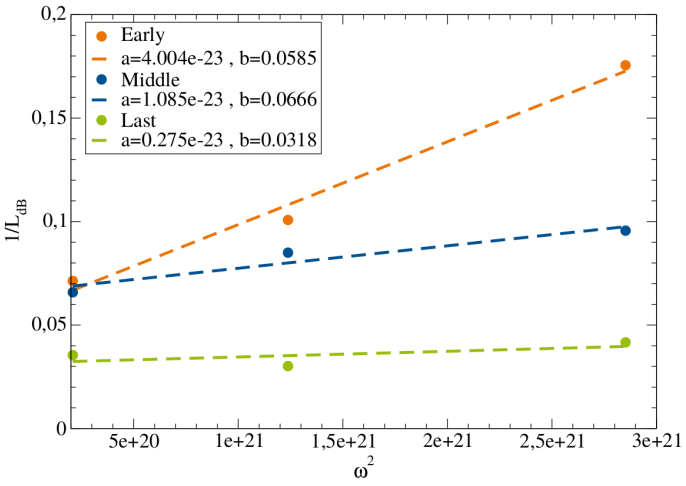

Figure 2: Lines $1/L_{dB}$ for three periods.

The curve $1/L_{dB}$ as a function of ω^2 is linear [15], and it is easy to obtain the parameters ω_p and ν_e from its slope a and its origin b (Figure 2).

$$\nu_e = \sqrt{\frac{b}{a}}\ ,\ N_e = \frac{1}{4.6 \cdot 10^{-5} y a \nu_e} \tag{7}$$

So we obtained: Table 1.

Table 1: Our parameters ν_e and ω_p obtained from the curve $1/L_{dB}$

	Early	**Middle**	**Last**
ν_e (s^{-1})	$38.22 \cdot 10^9$	$78.35 \cdot 10^9$	$107.53 \cdot 10^9$
ω_p (s^{-1})	$5.16 \cdot 10^9$	$6.92 \cdot 10^9$	$11.74 \cdot 10^9$

Our results of ω_p and ν_e are close to those given in Table 2 in [10]. The approximation (6) is valid, error are less than 2% (calculate on E/E_0).

Table 2: Error between the approximation L_{dB} (Eq. (6)) and the exact function (Eq. (4)).

Error (%)	Early	Middle	Last
2.3 GHz	1.3532	0.5914	1.7263
5.6 GHz	0.5305	0.4661	1.7436
8.5 GHz	0.2074	0.3155	1.3968

3.3. Numerical modelling

The plasma is modelled as a cylinder as shown in the configuration given by Figure 1. A time domain and a frequency domain approaches are used to describe attenuation of RF waves.

Both methods use a triangular mesh to discretize more accurately the computational domain. For the frequency domain computations, a Finite Element Method (FEM) is used. For the time domain computations, a nodal Discontinuous Galerkin (DG) method is used. This approach allows to determine through one simulation, the RF waves attenuation for a frequency band defined by the

transient incident signal. The DG method is suitable for high order spatial elements which allow to reduce dispersion error commonly encountered in FDTD methods, and to improve the solutions accuracy. An inverse Fourier transform is approximated in order to deal with the frequency dependence of electromagnetic parameters. The approximation uses a vector fitting technique [16] widely used in time domain modeling of dispersive media.

3.3.1. Frequency domain method

The symmetry of the system assumes to use half of the plasma and a Perfect Magnetic Conductor (PMC) boundary condition as shown in figure 3. The computational domain is surrounded by a Perfect Matched Layer (PML) of 1 m thickness. The spatial discretization in PML region is 5 elements per wavelength ($\lambda/5$) whereas it is 10 elements per wavelength ($\lambda/10$) elsewhere. The excitation is generated by a dipole located at the point S and the electric field is recorded at the point R.

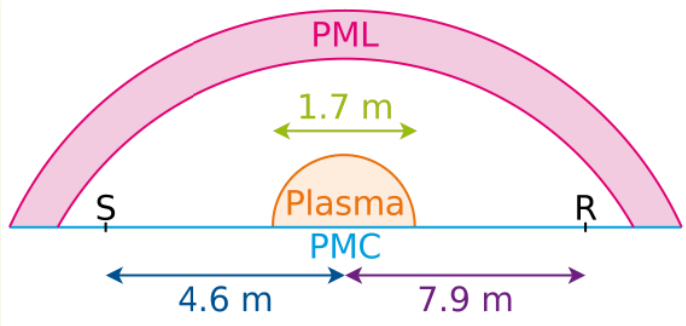

Figure 3: Box calculation for 2D FEM (Not to scale).

3.3.2. Time domain method

A time domain DG method based on upwind fluxes is assumed in this work. The simulation domain is delimited by an efficient PML recently proposed for time domain scattering problems [17]. In the initial mesh, the spatial discretization is PML region is 0.33 element per wavelength whereas it is 1 element per wavelength elsewhere. Elements of order $p = 8$ are used in these computations.

In this case the number of nodes in an element is given by $0.5(p+1)(p+2)$.

The simulations consist in propagating a modulated gaussian pulse with and without the plasma. This pulse is given by (8) with a frequency band between 0 and 10 GHz.

$$u(t) = \sin(2\pi f_0 t) \exp\left[-a(t-t_{ho})^2\right] \tag{8}$$

where $f_0 = 5.5$ GHz, $a = 2.4 \cdot 10^{19}$ s^{-1} and $t_{ho} = 7 \cdot 10^{-10}$ s.

3.4. Numerical results

Numerical results from FEM and DG computations are compared to those provided by Kinefuchi's works (Table 3 in [10]). We also added a comparison to analytical results obtained from $1D$ approximation [18] (Plasma is assumed to be a layer with a thickness of 1.7 m) and Mie series [19] (Plasma is assumed to be a cicular cylinder with a diameter of 1.7 m). The values obtained from these different methods are presented in Table 3.

The $1D$ results are very close to the experimental values because this model was used to compute the parameters ω_p and ν_e. The difference is due to the fact that the straight line is not passing by all the points.

Both DG and FEM results are validated by comparison to the Mie solution. Mie solution matches the experimental results except for the low frequency. In fact, the good agreement between numerical and experimental data is due to the validity of homogeneous parameters for high frequencies.

DG method allows to obtain the entire frequency band with one calculation thanks to a Fourier transform of the recorded field. On the other hand, the FEM requires a calculation of each frequency. We display all the results on a graph versus frequency for comparison (Figure 4).

The mean error calculation (relative to Mie) shows errors less than 1% for Early and Middle with FEM and less than 8% with DG. The error is greater for the Last period, less than 5% for FEM and less than 18% for DG. The high error obtained by the DG method is due to the increase of the relative error observed at low frequencies.

Table 3: Comparison of experimental and numerical values of normalized scattered field

Frequency	Method	Early	Middle	Last
	Exp	**0.199**	**0.174**	**0.039**
	FDTD	0.188	0.129	0.102
2.3 GHz	1D	0.174	0.187	0.028
(S-band)	Mie	0.250	0.271	0.147
	FEM	0.250	0.271	0.147
	DG	0.251	0.268	0.141
	Exp	**0.319**	**0.258**	**0.022**
	FDTD	0.310	0.200	0.034
5.6 GHz	1D	0.340	0.236	0.037
(C-Band)	Mie	0.303	0.196	0.021
	FEM	0.302	0.195	0.022
	DG	0.308	0.201	0.015
	Exp	**0.519**	**0.300**	**0.063**
	FDTD	0.424	0.241	0.024
8.5 GHz	1D	0.510	0.306	0.054
(X-Band)	Mie	0.510	0.298	0.072
	FEM	0.509	0.297	0.073
	DG	0.523	0.318	0.078

It is also observed that DG, FEM, Mie converge to the 1D solution when the frequency increases. This convergence shows that homogeneous parameters are even more acceptable if the frequencies are high. Therefore, high frequencies assumptions made in the 1D method, may allow to obtained a better estimation of the parameters for 2D calculations.

The plasma properties are largely determined by the electron number density and the ion collision frequency. The amount of electrons in a rocket motor plume can be influenced by many factors, including the propellant formulation, exhaust temperature, motor size, chamber pressure, light speed and altitude,

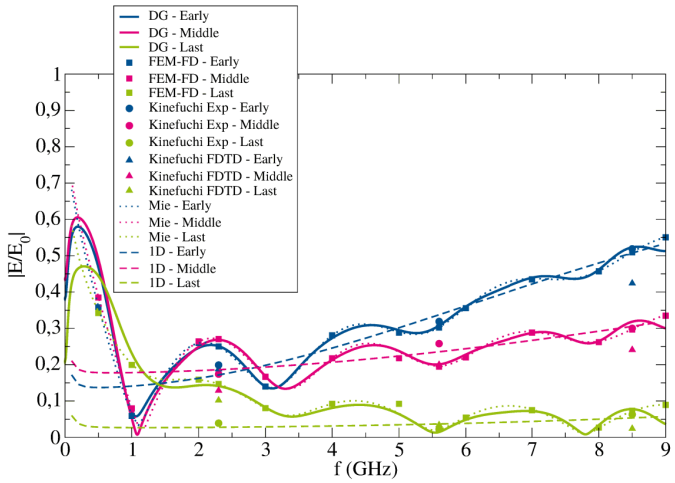

Figure 4: Comparison of calculation methods for the normalized scattered field versus the frequency.

and the distance down-stream from the nozzle exit Computational fluid dynamics is required to deduce the plasma properties but as far as the plasma can be described by an effective permittivity (equation (1)) the approach used in the paper remains valid. Similar plasma attenuation model can be found in [7]. The methods describe in 3.2 for obtained ω_p and ν_e from experiment and the method described in 3.3 with CFD for the ground configuration may be used by CNES in future work to validate CFD models.

4. In-flight attenuation estimation

In this section the finite element method in frequency domain (FEM) and an asymptotic method based on the diffraction theory are used to calculate attenuation of RF waves during a flight. In the asymptotic method the plume geometry is considered as a trapezium. The advantage of such approach is to avoid a memory-intensive calculation FEM and to allow a fast estimation of the attenuation. The main difficulty is the choice of the trapezium parameters. In this work we propose a new method TIP^3 (Trapezium Isovalues Permittivity Predict Parameter) to derive these parameters from a map of the permittivity.

4.1. Configuration study

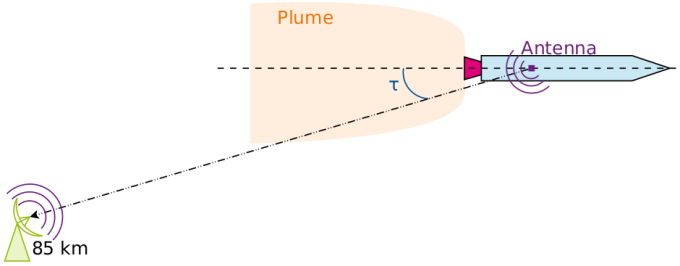

Figure 5: In-flight configuration. Launcher flies at 85 km of the ground antenna, τ is the look angle (Figure 1 in [5]).

The rocket studied in this work is the second stage of the MV-5 japanese solid-fuel launcher flight at 85 km of altitude [5]. A look angle τ is introduced to describe the configuration at each altitude (Figure 5).

Kinefuchi team performed CFD calculation deriving a map of ω_p and ν_e. Maps of ω_p and ν_e are extracted from Figure 17 in [5] and incorporate in FEM calculation (Figure 6).

In-flight measurement of the attenuation L_{dB} is carried out at the frequency 300 MHz (Figures 22 and 23 in [5], Pink points in figure 8).

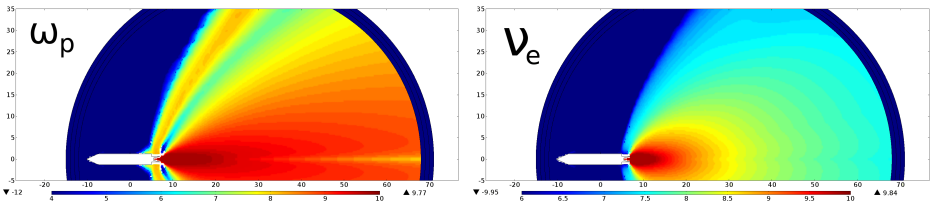

Figure 6: Map of $\log(\omega_p)$ and $\log(\nu_e)$ in calculation domain.

4.2. 2D Finite Element Method

The calculation domain is represented in figure 7.

The far-field calculation is used for reducing the size of the computational domain, because attenuation is measured at 85 km of the launcher.

A cardioids antenna is placed at $x = 7$ m of the nozzle exit and at $y = 1.25$ m (radius of launcher) of the launcher middle.

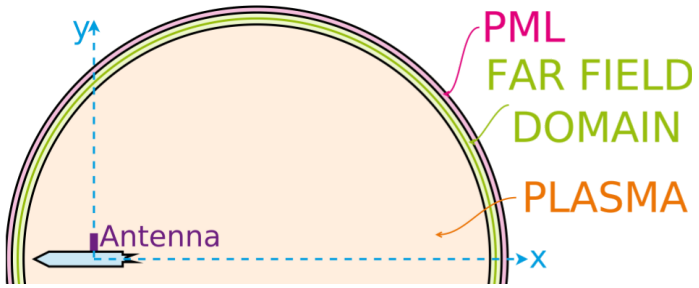

Figure 7: Geometrical representation. Pink zone correspond to the PML. Green zone correspond to a far-field computational domain. Orange zone correspond to the plasma. Radiuses of the arc are 40 m, 41 m, 42 m and 43 m.

The spatial discretization is 10 elements per wavelength ($\lambda/10$) and the domain is surrounded by a PML. The attenuation (in dB) is calculated and shown in figure 8.

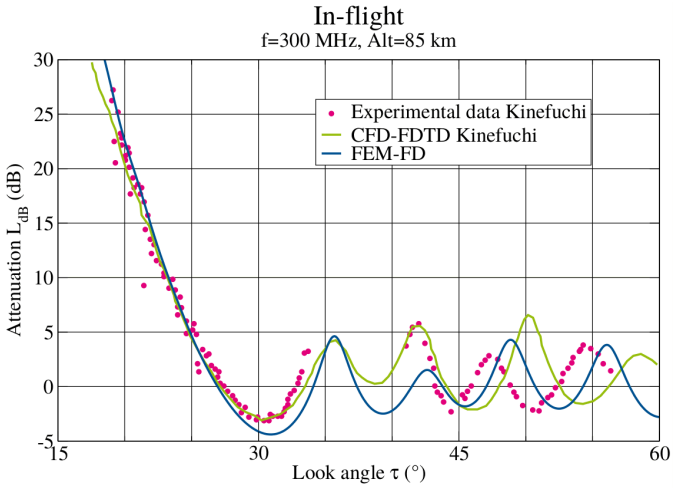

Figure 8: Attenuation obtained by FEM.

A good agreement is observed between FEM and experimental data. The differences might be due to the poor quality of map of ω_p and ν_e resulting from the literature.

4.3. Behavior of attenuation as a function of frequency

We perform simulations in frequency domain using the FEM method. The attenuation curves versus the look angle τ are shown for different frequency values in the figure 9.

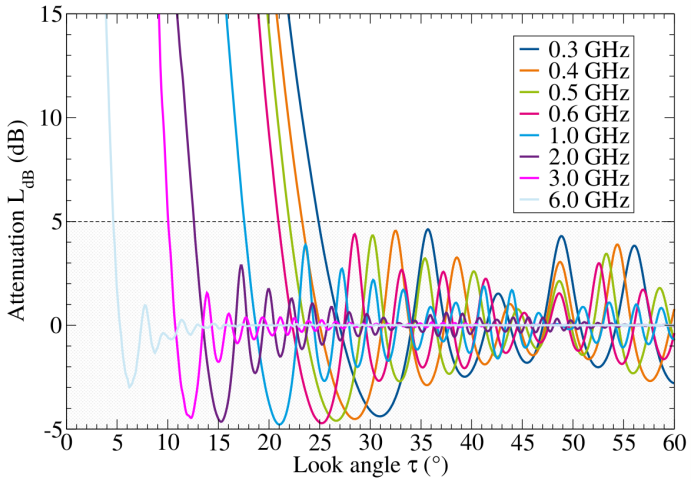

Figure 9: Attenuation in dB obtained by the FEM method for different frequency values.

These curves present a similar behavior. We remark a shift of the first minimum. After this first minimum, attenuations remain below 5 dB. So a good prediction of this minimum constitutes an interesting result. A statement of the look angle τ_{min} for which the first minimum occurs is shown in figure 10 (orange points). A linear regression (orange curve in figure 10, f are in GHz) is achieved and it shows a very good correspondence (all points are on the function): equation (9).

$$\tau_{min} = 20.9736 - 19.0258 \log(f) \tag{9}$$

This equation allows an immediate obtaining of τ_{min} for any frequency between 200 MHz and 6 GHz.

We sought to obtain analytic functions in order to predict the extrema of attenuation as a function of frequency, encouraged by the linear dependence of the first minimum.

We have identified seven specific angles as τ_{min}. An angle where the attenuation is about 20 dB (τ_{20}), another where the attenuation is about 10 dB (τ_{10}) (points on the slope), the two zeros around the first minimum (τ_{0_1} and τ_{0_2}), the first two minima (τ_{min} and τ_{min_2}) and the first maximum (τ_{max}).

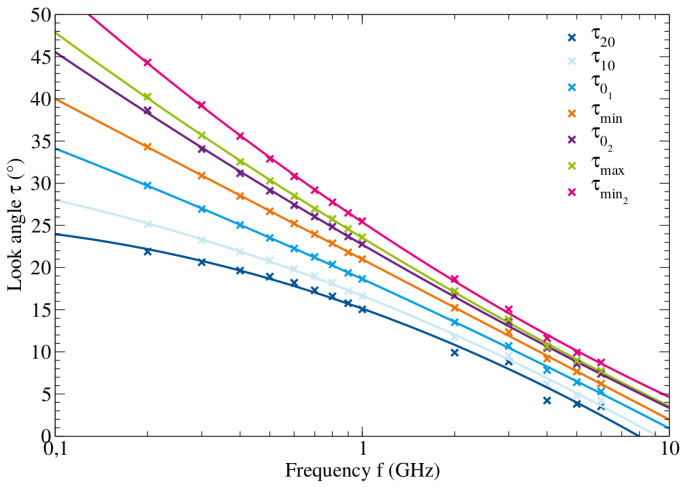

Figure 10: Look angles of interest.

Then, a linear function is sought as a function of frequency (f in GHz) for each angle of interest.

$$
\begin{aligned}
\tau_{20} &= 15.126 - 13.014\log(f) - 4.183\log(f)^2 \\
\tau_{10} &= 16.657 - 14.400\log(f) - 3.048\log(f)^2 \\
\tau_{0_1} &= 18.645 - 16.590\log(f) - 1.120\log(f)^2 \\
\tau_{min} &= 20.974 - 19.026\log(f) + 0.000\log(f)^2 \\
\tau_{0_2} &= 22.726 - 21.102\log(f) + 1.730\log(f)^2 \\
\tau_{max} &= 23.534 - 22.148\log(f) + 2.176\log(f)^2 \\
\tau_{min_2} &= 25.392 - 24.39\log(f) + 3.641\log(f)^2
\end{aligned}
\tag{10}
$$

This equations of the look angles allows an immediate obtaining of a schematic behaviour in frequency (between 200 MHz and 6 GHz) of attenuation L_{dB} (at least up to τ_{min_2}).

4.4. Impact of the antenna's position

We perform calculations with three antenna positions (12, 7 and 2 m) from the beginning of the plasma, at 300 MHz. The results are shown in figure 11.

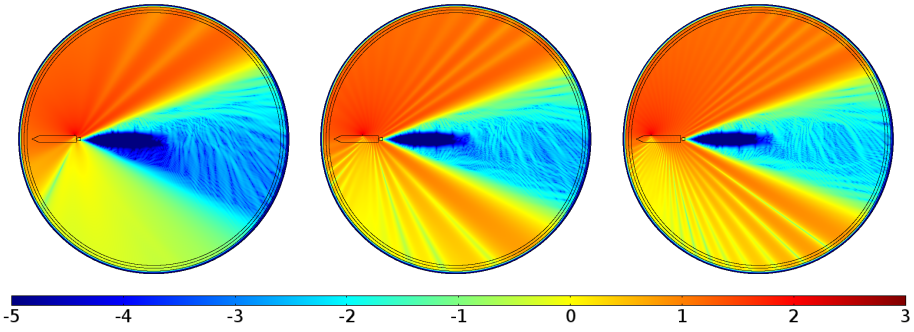

Figure 11: Electric field (log) at 300 MHz, antenna at 2, 7 et 12 m from plasma

A change in the distribution of the electric field is observed depending on the position of the antenna on the launcher. If the antenna is far away from the plasma, more interference fringes occur. The phenomenon is very marked for the antenna close to the plasma (2 m).

Note the presence of a weak electric field (cyan color) in the plasma in the case of remote antennas. What is less the case of the antenna close to the plasma, the electric field is much smaller (dark blue color) and crosses less the plasma.

The most credible explanation is that for the antenna close to the plasma, the electric field is directly diffracted by the plasma thus masking a part (less dense) of the plasma. Whereas if the antenna is further away the electric field can propagate before being diffracted thus reaching the previously hidden parts of the plasma.

4.5. Diffraction by a trapezoidal perfect conductor

We propose in this section an asymptotic method for the prediction of the far field. Trapezium parameters x_d, x_f, $\mathcal{C}_a$ and $\mathcal{C}_b$ are defined in figure 12.

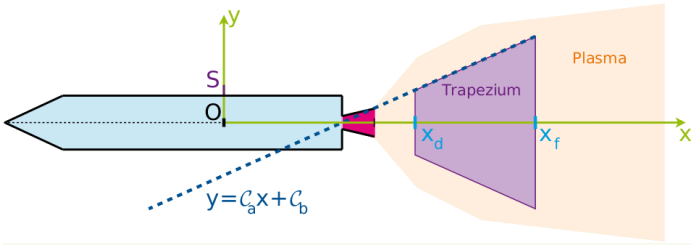

Figure 12: Trapezium characteristics x_d, x_f, $\mathcal{C}_a$ and $\mathcal{C}_b$.

4.5.1. Model

The asymptotic model predicts the far field in case where the plasma region is replaced by a perfectly conducting trapezium. The Huygens principle makes it possible to calculate the field diffracted by a perfectly conducting trapezium at point R illuminated by source placed at point S.

This method is based on [11] and also on [12], [13] and [14]. We show the principle of the method on a simple case and then we give the elements for the trapezium case.

Simple case – We consider a source at a point S and a conductive wall with height h placed at a distance s. The field at a point M placed at the distance x from O on the straight line defined by the conductive wall is given by:

$$E_M = E_S \int_h^\infty \exp\left(\imath \frac{2\pi}{\lambda} \Delta_M\right) \mathrm{d}x \tag{11}$$

where Δ_M is the optical path difference. It's a mathematical artefact! It is the integration of all points M which allows the resulting field to find a physical reality.

To have the field at the receiving point R located at the distance r:

$$E_R = E_M \int_h^\infty \exp\left(\imath \frac{2\pi}{\lambda} \Delta_R\right) \mathrm{d}x \tag{12}$$

where $\Delta_R = MR - OR$.

Finally, the field diffracted by a conductive plane is given by:

$$E = E_S \int_h^\infty \exp\left(\imath \frac{2\pi}{\lambda} \Delta\right) \mathrm{d}x \tag{13}$$

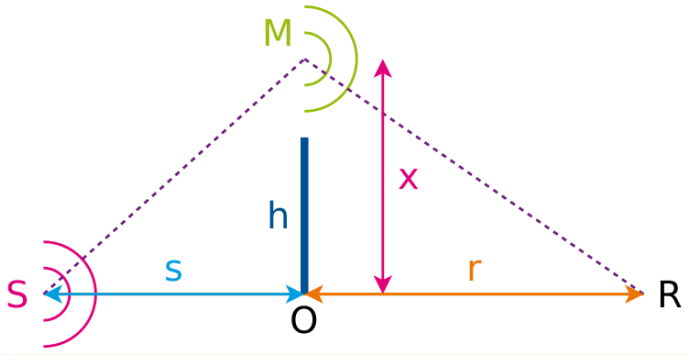

Figure 13: Simple case of diffraction method.

with $\Delta = SM + MR - SR$.

Trapezium – Similarly, on the trapezoid there are two possible paths, one taking into account the diffraction by the two conductive planes Δ_{SPQR} and the other taking into account the diffraction by the oblique surface Δ_{SPTQR}.

$$\Delta_{SPQR} = SP + PQ + QR - SR \tag{14}$$

$$\Delta_{SPTQR} = SP + PT + TQ + QR - SR \tag{15}$$

The diffracted field normalized by the two conductive planes is given by:

$$\left(\frac{E}{E_0}\right)_{dp} = -\frac{\imath}{2}\int_{h_2}\int_{h_1} \exp\left(\imath\frac{2\pi}{\lambda}\Delta_{SPQR}\right)\mathrm{d}x_1\mathrm{d}x_2 \tag{16}$$

The diffracted field normalized by the oblique conductive surface is given by:

$$\left(\frac{E}{E_0}\right)_{so} = -\frac{\imath}{2}\int_{h_2}\int_{h_1} \exp\left(\imath\frac{2\pi}{\lambda}\Delta_{SPTQR}\right)\mathrm{d}x_1\mathrm{d}x_2 \tag{17}$$

where:

$$\Delta_{SPQR} \approx \frac{x_1^2}{2a} + \frac{(x_2 - x_1)^2}{2b} + \frac{x_2^2}{2c} \tag{18}$$

$$\Delta_{SPTQR} \approx \frac{x_1^2}{2a} + \frac{x_2^2}{2c} + \frac{(x_2 + x_1)^2 - 4(h_1x_2 + h_2x_1) + 4h_1h_2}{2b} \tag{19}$$

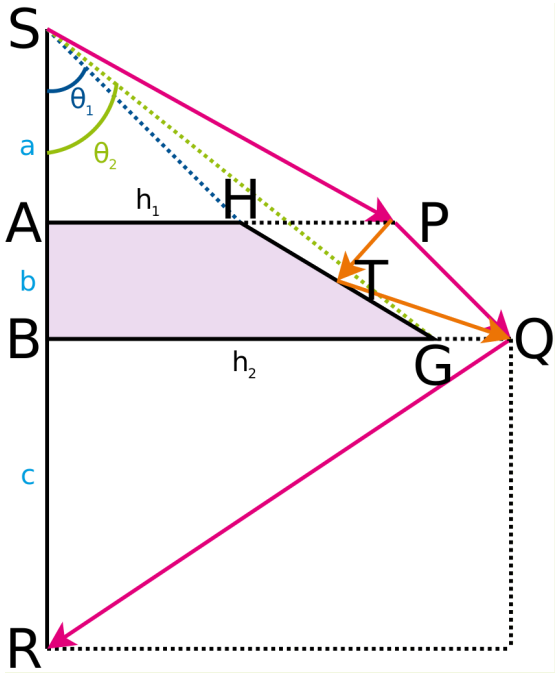

Figure 14: Configuration of the trapezium and optical paths. $AP = x_1$, $BQ = x_2$.

To solve the integrals, we use a change of variable in order to make appear the surface integral of Fresnel whose solution is known provided the surfaces are perfectly defined.

4.5.2. Methods TIP[3]

The objective is obtaining the trapezium characteristics directly from the permittivity. For beginning, the trapezium published in Kinefuchi's works [5] which have these properties is considered: $x_d = 20$ m, $x_f = 64$ m, $\mathcal{C}_a = 0.43$ and $\mathcal{C}_b = -2.61$. This trapezium is deduced from flight measurements. Unfortunately, in-flight measurements are quite difficult to get.

That is why the trapezium parameters are extracted from the map of the permittivity. So we compared the trapezium of Kinefuchi [5] and the cartography of permittivity (Figure 15).

We observed that the basis of the trapezium near to the launcher corresponds

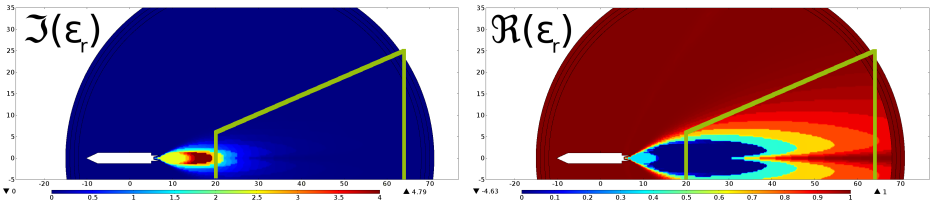

Figure 15: Comparison between Kinefuchi trapezium and permittivity. (Imaginary part $\Im(\varepsilon_r)$ and real part $\Re(\varepsilon_r)$

to a yellow colour in the representation of $\Im(\varepsilon_r)$. Either at a value of $\Im(\varepsilon_r) = 2.5$.

We also observed that the basis of the trapezium far to the launcher corresponds to a dark-orange colour in the representation of $\Re(\varepsilon_r)$. Either at a value of $\Re(\varepsilon_r) = [0.8 - 0.9] = 0.85$.

So isovalues of $\Im(\varepsilon_r) = 2.5$ and $\Re(\varepsilon_r) = 0.85$ are drawn and the correspondence between the adapted trapezium and the trapezium defined by these isovalues are confirmed (Figure 16).

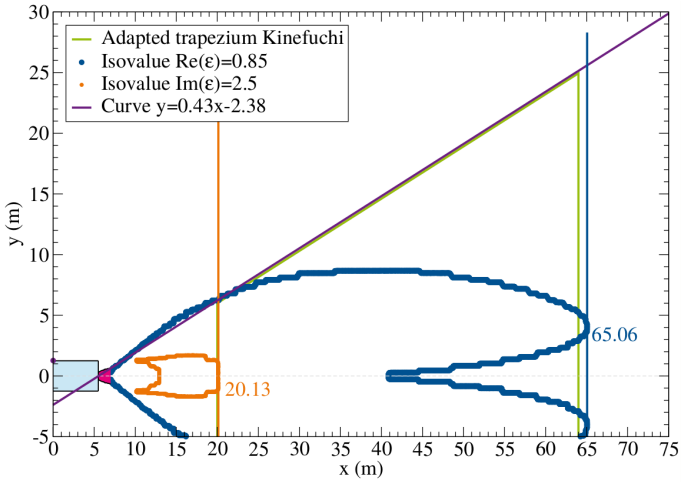

Figure 16: Comparison between the trapezium of Kinefuchi and the trapezium defined by isovalues of the permittivity.

The maximum values of x for isovalues $\Im(\varepsilon_r) = 2.5$ and $\Re(\varepsilon_r) = 0.85$, give x_d and x_f. The slope of the trapezium is determined by the line passing through the center of the throat and the end of the nozzle, so $\mathcal{C}_a = 0.43$ and $\mathcal{C}_b = -2.38$.

This method is generalized to all frequencies. x_d and x_f for all frequencies are determined with the use of the isovalues like made for 300 MHz. Next, a linear regression is done for obtained an analytical expression. The values x_d and x_f are given by:

$$x_d = -0.31 + 21.55\lambda^{0.50} \tag{20}$$

$$x_f = 1.54 + 69.65\lambda^{0.68} \tag{21}$$

The method TIP^{3}c is defined. This method gives the trapezium parameters: x_d by equation (20), x_f by equation (21), $\mathcal{C}_a = 0.43$ and $\mathcal{C}_b = -2.38$.

TIP^{3}c shows a significant difference in τ_{min} (Figure 17) compared to FEM. The method TIP^{3}p is defined to correct that. The parameter $\mathcal{C}_a$ is modified with the help of numerical result (FEM). A linear regression is made on $\mathcal{C}_a$ parameter on figure 17a and gives the equation (22).

The method TIP^{3}p gives the trapezium parameters: x_d by equation (20), x_f by equation (21), $\mathcal{C}_a$ by equation (22) where f are in GHz and $\mathcal{C}_b = -2.38$.

$$\mathcal{C}_a = 0.358 - 0.152\log(f) + 0.059\log(f)^2 \tag{22}$$

The values $\mathcal{C}_a$ and τ_{min} for methods TIP^3 and FEM are shown in figure 17.

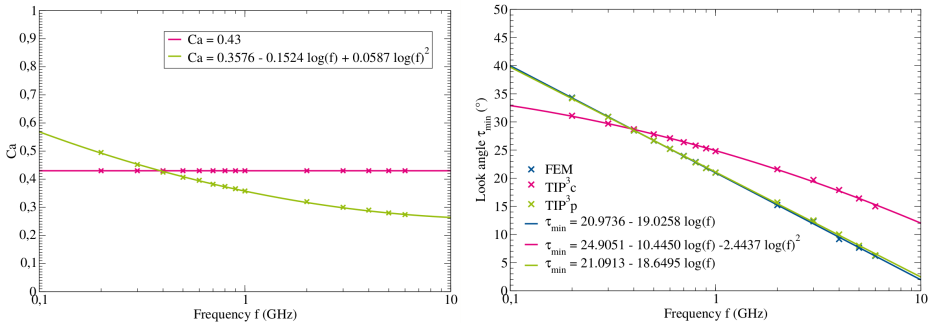

Figure 17: Expression of $\mathcal{C}_a$ and τ_{min}.

Pink curve (TIP^{3}c) corresponds to blue curve (FEM) with an error less than 5% in $f \approx [0.2 - 0.3]$ GHz. So the value $\mathcal{C}_a = 0.43$ given by the geometry of

the nozzle is correct for this frequency range. Green curve (TIP^{3}p) has an error less that 5% up to $f \approx 4$ GHz and also a error less than 1% up to $f \approx 1$ GHz

Some attenuation curves obtained from the FEM and the asymptotic methods using TIP^{3}p are shown in figure 18.

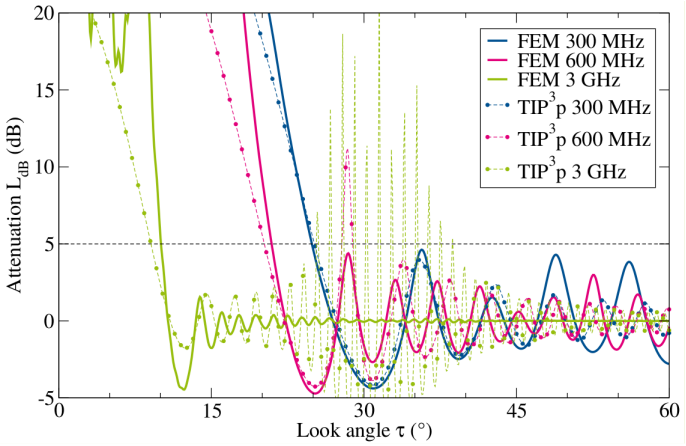

Figure 18: Attenuation at 300, 600 and 3 GHz.

A good angular behavior is reproduced by the TIP^{3}p method. Nevertheless an overestimation of the attenuation after the first minimum τ_{min} is noted for frequency values beyond 600 MHz. The FEM computations show that this attenuation is smaller than 5 dB for greater angles than τ_{min}. With the TIP^{3}p method, the variations of attenuation more than 5 dB can be ignored for the angles greater than τ_{min}.

Figure 19 show $\log_{10}(E/E_0)$ in plasma and TIP^{3}p perfectly conducting trapezium cases.

Interference fringe corresponding to the first minimum follow the slope of the trapezium. The trapezium serves as a mask increasing attenuation in the shadow. However the reflection at the corner of the trapezium scatters the field in the shadow of the trapezium thus modifying the slope of the attenuation for a low angle. The position of the bases cause the first interference fringe to follow the slope of the trapezium.

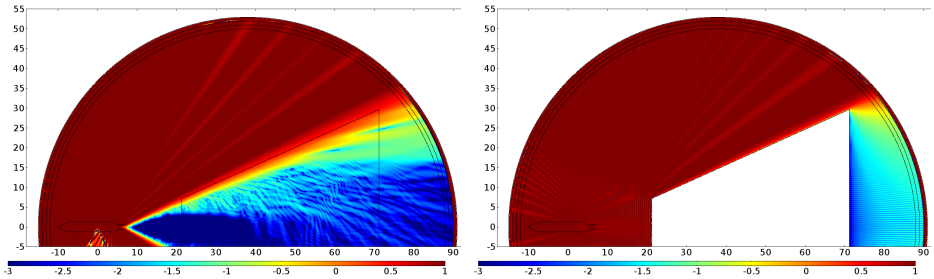

Figure 19: Comparison between normed electric field in presence of the plasma and the normed electric field in presence of the TIP^{3}p perfectly conducting trapezium at 300 MHz ($\log_{10}$).

5. Conclusion

In this paper the radio-frequency communication attenuation through a plasma rocket plume was studied using different methods. The analysis of the ground experiment revealed the importance of the attenuation phenomena through the plasma. A frequency-domain finite element method (FEM) and a time domain discontinuous Galerkin method (DGTD) provided a good estimation of the attenuation. In the case of the launcher in flight, attenuation of RF communications is computed by the FEM method using maps of ω_p and ν_e from the literature. To face problem of the heavy computational time that occurs with FEM approach for high frequencies, an asymptotic technique is presented. It is proposed when the shape of the plume is considered as a trapezium whose parameters are deduced from the knowledge of the permittivity distribution (TIP^{3}p). A complete validation was proposed for a wide range of frequency values.

References

[1] R. R. Mikatarian, C. J. Kau, H. S. Pergament, Fast computer program for nonequilibrium rocket plume predictions, Defense technical information center Accession No. AD0751984 (1972) 1–20.

[2] L. D. Smoot, D. L. Underwood, Prediction of microwave attenuation char-

acteristics of rocket exhausts, AIAA 6th solid propellant rocket conference 65-181 (1965) 1–60. doi:10.2514/6.1965-181.

[3] L. D. Smoot, T. J. Seliga, Rocket exhaust plume radar attenuation and amplitude/phase noise, J. Spacecraft 4 (1967) 774–780. doi:10.2514/3.28950.

[4] J. A. Blevins, R. A. Frederick, H. W. Coleman, An assessment of microwave measurement techniques in rocket exhaust applications, 32nd aerospace sciences meeting & exhibit 94-0671 (1994) 1–9. doi:10.2514/6.1994-671.

[5] K. Kinefuchi, K. Okita, I. Funaki, T. Abe, Prediction of in-flight radio frequency attenuation by a rocket plume by applying CFD/FDTD coupling, 49th AIAA/ASME/SAE/ZSEE Joint Propulsion Conference 2013-3790 (2013) 1–20. doi:10.2514/6.2013-3790.

[6] L. G. McMillion, A simple method for predicting RF attenuation through a rocket exhaust plume, Defense technical information center Accession No. ADA443181 (1997) 1–15.

[7] B. van der Veek, S. Chintalapati, D. R. Kirk, H. Gutierrez, R. F. Bun, Modeling and validation of ku-band signal attenuation through rocket plumes, Journal of Spacecraft and rockets 50 (2013) 992–1001. doi:10.2514/1.A.32358.

[8] B. Fromentin-Denozière, D. Gueyffier, J. Simon, Numerical modelling of the radar signature of rocket exhaust plumes, International Conference on Electromagnetics in Advanced Applications (ICEAA 2012) (2012) 400–403doi:10.1109/ICEAA.2012.6328658.

[9] K. Kinefuchi, I. Funaki, T. Abe, Frequency-dependent FDTD simulation of the interaction of microwaves with rocket-plume, IEEE Transactions on antennas and propagation 58 (2010) 3282–3288. doi:10.1109/TAP.2010.2055796.

[10] K. Kinefuchi, I. Funaki, H. Ogawa, T. Kato, S. Tachikawa, T. Shimada, T. Abe, Investigation of micromawe attenuation by solid rocket exhausts, 47th AIAA Aerospace Science Meeting and Exhibit 2009-1386 (2009) 1–10. doi:10.2514/6.2009-1386.

[11] K. Kinefuchi, I. Funaki, T. Abe, Prediction of in-flight frequency attenuation by rocket plume applying diffraction theories, Journal of spacecraft and rockets 50 (2013) 150–158. doi:10.2514/1.A32223.

[12] J. H. Whitteker, Diffraction over flat-topped terrain obstacle, IEE proceedings 137 (1990) 113–116. doi:10.1049/ip-h-2.1990.0021.

[13] G. Millington, R. Hewitt, F. S. Immirzi, Double knife-edge diffraction in field-strength predictions, Proceedings IEE 507 (1962) 419–429. doi:10.1049/pi-c.1962.0059.

[14] G. Millington, R. Hewitt, F. S. Immirzi, The Fresnel surface integral, Proceedings IEE 508 (1962) 430–437. doi:10.1049/pi-c.1962.0060.

[15] K. M. Mphale, P. V. Luhanga, M. L. Heron, Microwave attenuation in forest fuel flames, Combustion and flame 154 (2008) 728–739. doi:10.1016/j.combustflame.2008.07.006.

[16] B. Gustavsen, A. Semlyen, Rational approximation of frequency domain responses by vector fitting, IEEE Trans. Power Delivery 14 (1999) 1052–1061. doi:10.1109/61.772353.

[17] A. Modave, A. Kameni, J. Lambrechts, E. Delhez, L. Pichon, C. Geuzaine, An optimum pml for scattering problems in the time domain, Eur. Phys. J. Appl. Phys. 64 (2013) 24502. doi:10.1051/epjap/2013120447.

[18] E. Dieudonné, N. Malléjac, C. Amra, S. Enoch, Surface and bulk scattering by magnetic and dielectric inhomogeneities: a first-order method, J. Opt. Soc. Am. A 30 (2013) 1772–1779. doi:10.1364/JOSAA.30.001772.

[19] J. V. Bladel, Electromagnetic fields, John Wiley & Sons, 2007.